Roughness-induced friction in liquid foams

Manon Marchand, Frederic Restagno, Emmanuelle Rio, François Boulogne

Roughness-induced friction in liquid foams

Manon Marchand[1], Frédéric Restagno[1], Emmanuelle Rio[1], and François Boulogne[1]

[1]Université Paris-Saclay, CNRS, Laboratoire de Physique des Solides, 91405, Orsay, France

February 10, 2020

Abstract

Complex liquids flow is known to be drastically affected by the roughness condition at the interfaces. We combined stresses measurements and observations of the flow during the motion of different rough surfaces in dry liquid foams. We visually show that three distinct friction regimes exists: slippage, stick-slip motion, and anchored soap films. Our stress measurements are validated for slippage and anchored regimes based on existing models, and we propose a leverage rule to describe the stresses during the stick-slip regime. We find that the occurrence of the stick-slip or anchored regimes is controlled by the roughness factor, defined as the ratio between the size of the surface asperities and the radius of curvature of the Plateau borders.

The flow of complex fluids – polymers [1, 2], emulsions [3], granular materials [4, 5], bubbly liquids [6], foams [7, 8] – near a solid surface displays different behaviors depending on the surface properties. Often, these systems exhibit a slippage on smooth surfaces but deform and flow on rough surfaces. Therefore, asperities are commonly added on the measurement apparatus to suppress the interfacial dissipations [9, 10, 11]. Here, we focus our study on the flow of foams for which the elementary elements, the bubbles, can be observed directly.

The friction of an elongated bubble in a smooth round capillary has been studied in the pioneering work of Bretherton at low capillary numbers $\mathrm{Ca} = \mu V/\gamma$, where μ and γ are the dynamic viscosity and air-liquid surface tension of the solution, and V is the meniscus velocity in the capillary [12]. It is shown experimentally and theoretically that the stress follows a $\mathrm{Ca}^{2/3}$ power law. This prediction is also valid for a single bubble in a flat cell [13], and can be extended for foams [14]. The surface rheology of the foaming solution influences the power law, but in this study we work with a solution for which this issue is negligible [14, 15]. Also, experimental measurements provide a correction accounting for the liquid fraction of the foam φ_ℓ [16].

In rheology, the wall slippage of the probed material must be avoided to ensure that the dissipation is localized in the bulk of the sample. In the case of foams, a commonly adopted rule-of-thumb to prevent slippage consists in adding asperities larger than the bubble size on the walls [17], and to assert either visually [18] or by showing that the rheological measurements do not depend on the confinement [15, 10], that there is no remaining slippage. This trial and error process is not always possible and the characterization of the effect of different roughness sizes has been studied for single wet bubbles on walls [6], but not for dry liquid foams.

In this Letter, we explore systematically the effect of different sizes of wall asperities a on the flow of dry liquid foams and we identify three friction regimes at zero, high or intermediate roughness. The contribution of the roughness size a, of the liquid fraction φ_ℓ, and of the inserting velocity in the foam V to the stresses are rationalized in each regime. The roughness size is shown to change the stresses over one order of magnitude. We show that the roughness factor a/r_{pb} is a single criterion for the crossover between wall and bulk dissipation regimes. Interestingly, this parameter is independent of the imposed velocity.

Our experiment consists in inserting horizontally a controlled rough surface in a dry monodisperse foam generated in a transparent container (Fig. 1a and b). We produce the foam by blowing air through needles in a foaming solution. The obtained bubble radius is $R = 0.70 \pm 0.05$ mm, and the liquid fraction φ_ℓ of the foam can be varied between 0.03 and 8 % by changing the working height above the liquid-foam interface [19] (Fig. S2). For such dry foams, the radius of curvature of the Plateau borders is given by $r_{\mathrm{pb}} = R\sqrt{\varphi_\ell/0.33}$ [20]. It varies in the range $0.02 - 0.4$ mm in our experiment. Model rough surfaces are obtained by gluing glass beads of mean radii a on microscope glass slides (Fig. S1), Fig. 1a). We insert the surfaces in foams at constant velocities V from 0.5 to 20 mm/s, corresponding to capillary numbers Ca in the range 1.7×10^{-5} to 6.7×10^{-4}. Simultaneously, we measure the tangential force F exerted by the foam on the surface (Fig. S3).

By tracking the position of the Plateau borders p_{pb} in contact with the patterned surface during the motion, we identify three distinct friction regimes (Fig. 1d), which are discriminated by the dimensionless roughness factor a/r_{pb}. The emergence of this parameter can be intuited. When a bead is smaller than the size of the Plateau border r_{pb}, it enters the Plateau border and slides inside it whereas bigger beads experience a pinning force at the liquid air interface (Fig.2e). For negligible roughness sizes compared to the characteristic size of a Plateau border, $a \ll r_{\mathrm{pb}}$, the Plateau borders slide on the solid surface (Supplementary Movie S1). For $a \sim r_{\mathrm{pb}}$, Plateau borders are anchored on the surfaces but occasionally jump back (Supplementary Movie S2), while for $a \gtrsim r_{\mathrm{pb}}$ Plateau borders remain anchored and the stress is released by plastic events between bubbles in the bulk of the foam (Fig. 1d, e, Supplementary Movie S3). We will respectively refer to these regimes as sliding, stick-slip, and anchored regimes in the following discussion. For a/r_{pb} between 1 and 3, the visualizations reveal that the stress is released by mixed slip or plastic events. This provides a first estimate of the transition between the stick-slip regime and the anchored one.

Typical force measurements as a function of time t, or equivalently of the position of the surface p, are presented for each regime in Fig. 1c. The linear evolution of the force

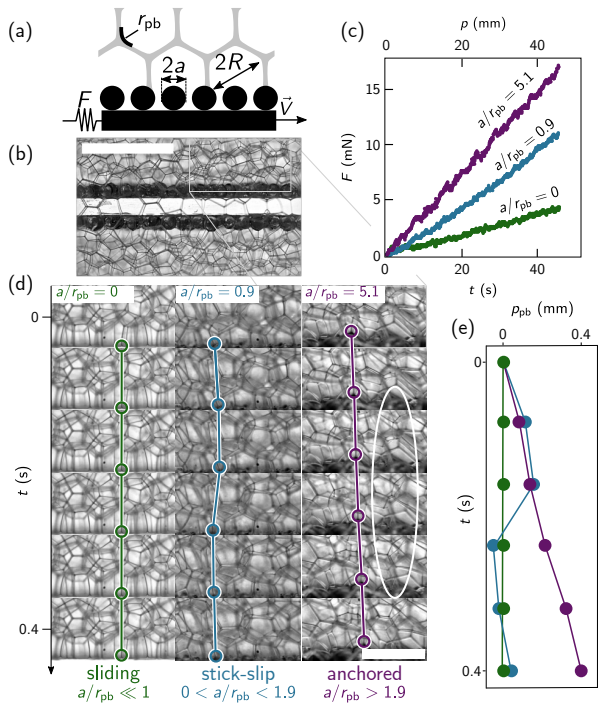

Figure 1: Foam flow dynamics near a solid surface decorated with glass beads. (a) Side view of the surface of roughness size a moving at constant speed V in a foam of bubble radius R and radius of curvature of Plateau borders r_{pb}. The force F exerted by the foam on the surface is recorded. (b) Photograph corresponding to the schematic (a). The scale bar is 5 mm. (c) Raw force measurements as a function of time t and position of the surface p for one smooth and two patterned surfaces translating at $V = 1$ mm/s from left to right. (d) Visualization of the Plateau borders in contact with the patterned surfaces for three different a/r_{pb}. The bottom of each picture is the surface moving at 1 mm/s. We mark the position p_{pb} of a Plateau border with a circle. A plastic event is circled in white. The scale bar represents 2 mm. (e) Position of the Plateau borders p_{pb} for the three friction regimes, reported from (d).

indicates that the probed phenomena are independent of the penetration depth of the surface, and that a constant stress value τ_{p} can be extracted from $F(t)$ and $p(t)$ for each experiment (Fig. S5).

We reproduce the experiment for various roughness sizes a, radius of curvature of Plateau borders r_{pb}, and insertion velocities V. In Fig. 2a, we plot the stress τ_{p} as a function of the roughness factor a/r_{pb}. The different point colors represent the three regimes identified from the images. In this representation, the data for a single velocity collapses on a trend curve (Fig. S4). Complementary representations of the stick-slip and the anchored regimes presenting the influence of the asperity size a and the velocity V are provided in Fig. S7. Interestingly, tuning a/r_{pb} leads to a stress variation of about an order of magnitude, which highlights the crucial effect of the boundary conditions on stresses. In the following, we examine each regime to rationalize the dynamics.

The sliding regime, for which $a \ll r_{\mathrm{pb}}$, has already been investigated [12, 16, 14], and these studies validate experimentally that the stress at the solid wall can be written

$$\tau_{\mathrm{slip}} = 3.8\frac{\gamma}{R}\varphi_\ell^{-0.25}\mathrm{Ca}^{2/3}. \qquad (1)$$

In Fig. 2b, the stress measurements are plotted as a function of the prediction given by equation (1), which shows a good agreement and validates this experimental approach.

Now, we consider the anchored regime for the large roughness factors. The common description of the foam rheology suggests that for shear stresses lower than a yield stress τ_{ys}, the foam behaves as an elastic solid, whereas for stresses exceeding the yield stress, the foam flows. Phenomenologically, this behavior is described by a Hershell-Bulkley law $\tau_{\mathrm{HB}} = \tau_{\mathrm{ys}} + \eta(\dot\gamma)\dot\gamma$, where $\dot\gamma \sim V/\delta$ is the shear rate that scales as the velocity over a characteristic shear length δ and $\eta(\dot\gamma)$ is the effective foam viscosity that depends on $\dot\gamma$ [21, 11]. The ratio of the yield stress and the viscous term defines the Bingham number $\mathrm{Bi} = \frac{\tau_{\mathrm{ys}}}{\eta(\dot\gamma)\dot\gamma}$ [22]. The yield stress value is described by a semi-empirical law $\tau_{\mathrm{ys}} = K\frac{\gamma}{R}(\varphi_{\mathrm{c}} - \varphi_\ell)^2$, where $\varphi_{\mathrm{c}} = 0.26$ is the fraction of gaps remaining in a close-packing of hard spheres [19], and K is a proportionality factor which reported values vary between 0.5 and 6 [23, 24]. Since we are working with dry foams, we have $\varphi_\ell \ll \varphi_{\mathrm{c}}$, which leads to

$$\tau_{\mathrm{ys}} = K\frac{\gamma}{R}\varphi_{\mathrm{c}}^2. \qquad (2)$$

In the limit of low velocities, corresponding to $\mathrm{Bi} > 1$, the contribution of the yield stress is dominant (see SI). The Fig. 2d shows that the stress applied by the foam on the rough surfaces is nearly independent on the velocity and its value is predicted by the equation (2) with a prefactor $K = 2.9 \pm 0.3$, which is in agreement with previously recorded values [23, 24]. We notice that the measured stress increases slightly for the larger velocities, which is reminiscent of the viscous term in the Hershell-Bulkley model.

Up to this point, we analyzed the two extreme limits of negligible and large dimensionless roughness factor a/r_{pb}. For roughness sizes comparable to the radius of the Plateau borders, we observe a stick-slip regime that has been observed but not characterized [25], to the best of our knowledge. Our experiments indicate that the transition between the stick-slip and the anchored regimes is continuous (Fig. 2a). This suggests that the stick-slip regime is a combination of sliding, where the energy is released by viscous dissipation in the Plateau borders, and anchoring, where the energy is stored by deforming elastically the foam.

In the stick-slip regime, (Fig. 2e) an asperity moving in a foam goes through the liquid air interface of a Plateau border over a duration $t_{\mathrm{anchored}} \propto a/V$, experiencing a pinning force. Then, the asperity moves inside the Plateau border over a typical duration $t_{\mathrm{slip}} \propto r_{\mathrm{pb}}/V$. Therefore, we introduce the ratio of these durations, $\tilde a = a/kr_{\mathrm{pb}}$, where the prefactor k represents the value of the transition. This two-step description happens for each asperity on the whole probing surface. The stick-slip events are not occurring simultaneously (Supplementary Movie S2), thus we average the individual behaviors of the Plateau borders. Hence, we construct a leverage rule stating that the total stress is the sum of the contributions of a pinning stress for a relative duration $\tilde a$ and of a viscous stress for the complementary relative duration $(1 - \tilde a)$. This writes

$$\tau_{\mathrm{stick-slip}} = \tau_{\mathrm{ys}}\tilde a + \tau_{\mathrm{slip}}(1 - \tilde a). \qquad (3)$$

To determine more precisely the value of the transition k, we optimized equation (3) against this parameter and we obtained a transition at $k = 1.9 \pm 0.2$ (Fig. S6a). This value of

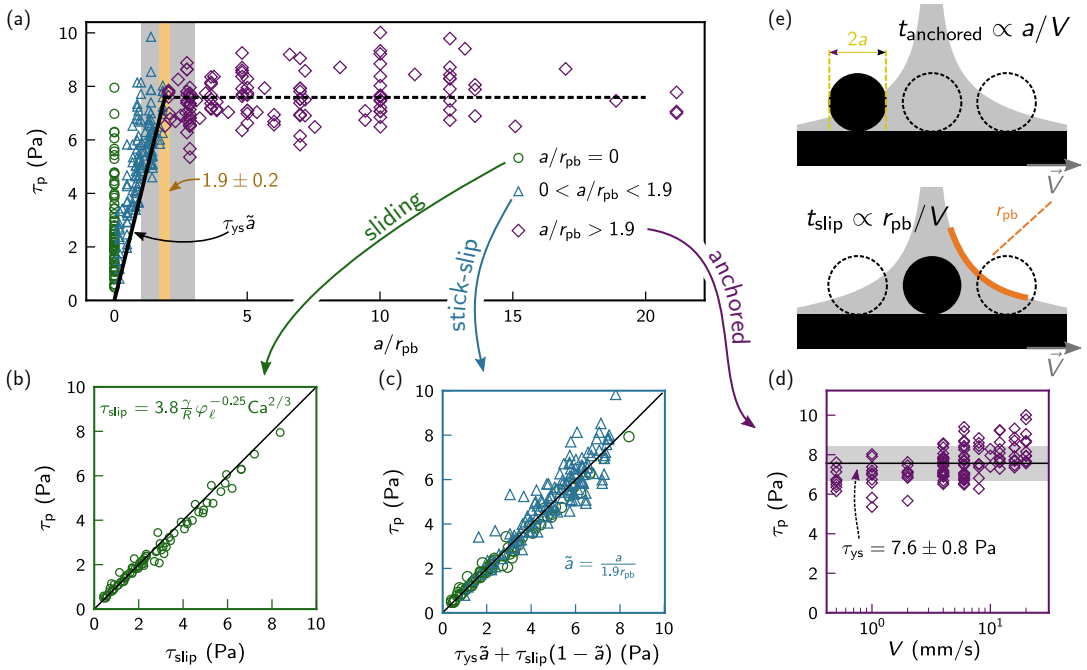

Figure 2: Stress measurements and identification of the three friction regimes. (a) Stress τ_p obtained from the force measurements as a function of the roughness factor a/r_{pb}. The solid black line represents the equation (3) for $V \to 0$, and the dashed black line is τ_{ys} with $K = 2.9$. The gray area shows the transition between the stick-slip and the anchored regime as deduced from observation of the videos, and the orange area is the transition obtained by optimizing k in Eq. (3). (b) For $a/r_{pb} = 0$, stress measurements as a function of the equation (1). (c) Stress values for the sliding (green circles) and the stick-slip (blue triangles) conditions, as a function of equation (3). (d) In the anchored regime, measured stresses as a function of the imposed velocity V. The solid line is the mean of all stresses τ_{ys} and the gray area represents the standard deviation. The deviation for the higher velocities indicates a more significant contribution of the viscous term in the Hershell-Bulkley model. (e) Schematics of a Plateau border moving on a rough surface. The beads spend a time proportional to a/V going through the liquid air interface, and a time proportional to r_{pb}/V in the bulk of the Plateau border.

order unity is in agreement with our estimation of the transition from direct visualizations of the Plateau border dynamics (see the orange and gray areas in Fig. 2a). As shown in Fig. 2c, the proposed equation (3) is in excellent agreement with the stress measurements for the different liquid fractions and surface velocities explored in this study. In the vicinity of small velocities, we expect $\tau_{stick-slip} \underset{V\to 0}{\to} \tau_{ys}\tilde{a}$, and this is observed in Fig. 2a and Fig. S6b.

Thus, we identified a practical criterion $\tilde{a}$ to discriminate between surface and bulk dissipation for the friction of a foam on a solid surface. The anchored regime is of particular interest for rheological studies focusing on the flow of foams where a no slip condition is necessary to transfer shear to the bulk of the material. It was already known that adding some asperities by gluing sand paper or engraving grooves on a measuring apparatus reduces the wall slippage [17], but the size of these asperities had not been tuned systematically. Our study validates this approach, since the stress in the anchored regime are independent of the size of the asperities beyond a critical roughness factor (Fig. 2a). When the grit size of the sand paper is insufficient to totally eliminate the wall slippage, the mixed surface and bulk dissipation leads to a difficult interpretation of the data [8]. Differences in the measured stresses are also reported when the grit size is increased [26]. This behavior is likely the stick-slip regime we report in Fig. 2c. Our contribution allows one to choose a suitable roughness to be added on the measuring systems regarding the foam properties. The results then assess that the obtained measurements in the anchored regime will be uncorrelated with the size of the roughness.

The stick-slip regime allows, for instance, to understand the mastication of an aerated food (Fig. 3a). Adding air bubbles in a food product affects mouthfeel perception, improves digestibility, and aids mastication [27]. In the case of eating disorders, such as dysphagia, more viscous foods are proven to be safer [28]. With viscosities typically 10^3 times bigger than the viscosity of water [29], foams could help patients. We make a visualization experiment to illustrate the tunability of perception during the mastication of a foamed food. Human tongue asperities have a fixed size, therefore the remaining adjustable parameters in this case are the bubble size and the liquid fraction of the foam. A glass slide covered with asperities of mean radius $a = 225$ μm, a size comparable to human papillae [30], can be considered as a model human tongue (Fig. 3a, b and c). We produce two edible albumen foams with a bubble size $R = 0.7$ mm and two different liquid fractions, using the same technique than soap foams, but with a solution containing 1 g of egg white powder (Louis François) and 200 mL of deionized water. The two foams are sheared between a table spoon moving at 10 mm/s and the static model tongue. In the two cases, the last bubble is circled to illustrate the slippage of the foam (Fig. 3d). For the wetter foam for which $\tilde{a} \simeq 0.5 < 1$, the conditions predict a stick-slip regime and the foam moves on the surface (Supplementary Movie S4), whereas for the dryer foam, for which $\tilde{a} \simeq 3 > 1$, the foam sticks to the surface (Supplementary Movie S5). This illustrates that the results of our controlled

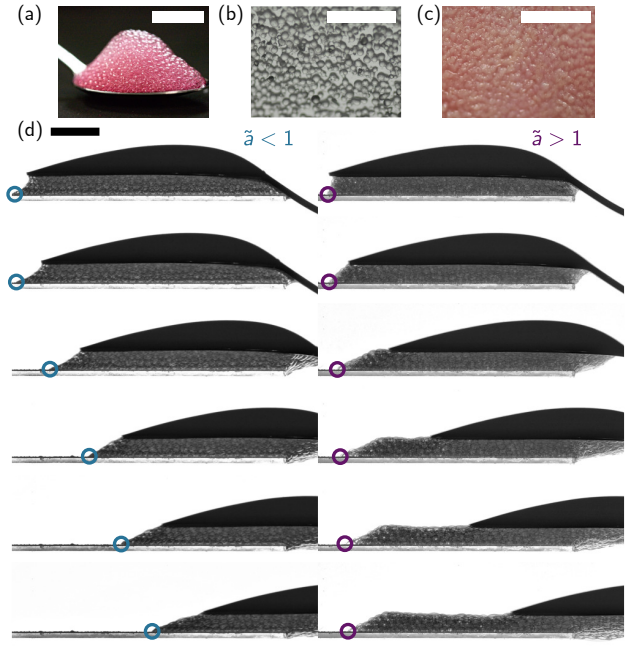

Figure 3: Edible foams and texture sensation. (a) Albumen foam in a spoon. The scale bar is 1 cm. A drop of food dye is added for visualization. (b) Rough surface with beads of mean radius $a = 225$ μm. The scale bar is 5 mm. (c) Close up picture that shows the papillae on a human tongue. The scale bar is 5 mm. (d) Albumen foam sheared between a table spoon and a glass surface covered with beads of mean radius $a = 225$ μm. The left side is a wet foam with $\varphi_\ell \simeq 0.7$ %, corresponding to $\tilde{a} \simeq 0.5$. The right side is a dryer foam with a liquid fraction $\varphi_\ell \simeq 0.02$ %, meaning $\tilde{a} \simeq 3$. In those two cases the last bubble on the surface is circled to enlighten the motion of foam on the model tongue. There is a 1 s interval between two consecutive images. The scale bar is 1 cm.

experiment are valid in a more general context, with different shearing geometries and surfactants. When the normalized roughness $\tilde{a}$ varies from 0 to 1 in the stick-slip regime, we see in Fig. 2a that the stress varies between 0.8 and 9.8 Pa, a range of stresses detectable by a human tongue [31, 32]. Thus, tuning the macroscopic properties of a product, namely the bubble size and the liquid-gas ratio, must lead to different sensations in mouth.

In conclusion, we reveal that the foam flow near surfaces exhibit different behaviors: sliding, anchored, and stick-slip. By recording the stresses exerted during these regimes, we show that there exists a roughness, normalized by the curvature radius of the Plateau borders of the foam, $\tilde{a} = a/kr_{\rm pb}$ beyond which the dissipation is transferred from the surface to the bulk. This transition does not depend on the imposed velocity in the explored range. In the stick slip regime, we propose a leverage rule describing the influence of speed, radius of curvature of Plateau borders, and liquid fraction on the stresses exerted on the walls. We measure that these stresses vary on one order of magnitude when the normalized roughness is increased. Therefore, we contribute to an improved description of wall roughness effect on flowing foams, which is of particular interest to design surfaces given the foam properties in industrial applications. In contrast, when surface asperities are unchangeable, as in the case of tongue papillae, our description of friction forces allows to finely tune the properties of edible foams to get creamy or gooey mouth feelings. This is useful for inventing new foamed food products, either for the ease of feeding for dysphagic patients, or for the gourmets' pleasure.

Acknowledgements M.M. acknowledges EDPIF for funding support. We thank J. Sanchez for programming the computer interface of the experiment, and G. Guillier for support manufacturing the force sensor. We thank B. Dollet and C. Raufaste for discussions.

References

[1] R. D. Priestley, C. J. Ellison, L. J. Broadbelt, and J. M. Torkelson. Structural relaxation of polymer glasses at surfaces, interfaces, and in between. *Science*, 309(5733):456–459, 2005.

[2] P. E. Boukany, O. Hemminger, S.-Q. Wang, and L. J. Lee. Molecular imaging of slip in entangled dna solution. *Phys. Rev. Lett.*, 105:027802, 7 2010.

[3] J. Goyon, A. Colin, G. Ovarlez, A. Ajdari, and L. Bocquet. Spatial cooperativity in soft glassy flows. *Nature*, 454(7200):84—87, 7 2008.

[4] S. Siavoshi, A. V. Orpe, and A. Kudrolli. Friction of a slider on a granular layer: Nonmonotonic thickness dependence and effect of boundary conditions. *Phys. Rev. E*, 73:010301, 1 2006.

[5] O. Pouliquen. On the shape of granular fronts down rough inclined planes. *Physics of Fluids*, 11(7):1956–1958, 1999.

[6] D. Germain and M. Le Merrer. Bubbles slipping along a crenelated wall. *EPL*, 115(6):64005, 2016.

[7] A. Kabla and G. Debrégeas. Local stress relaxation and shear banding in a dry foam under shear. *Phys. Rev. Lett.*, 90:258303, 6 2003.

[8] K. Golemanov, S. Tcholakova, N. D. Denkov, K. P. Ananthapadmanabhan, and A. Lips. Breakup of bubbles and drops in steadily sheared foams and concentrated emulsions. *Phys. Rev. E*, 78:051405, 11 2008.

[9] H. A. Barnes. A review of the slip (wall depletion) of polymer solutions, emulsions and particle suspensions in viscometers: its cause, character, and cure. *Journal of Non-Newtonian Fluid Mechanics*, 56(3):221 – 251, 1995.

[10] M. Cloitre and R. T. Bonnecaze. A review on wall slip in high solid dispersions. *Rheologica Acta*, 56(3):283–305, 3 2017.

[11] S. Cohen-Addad, R. Höhler, and O. Pitois. Flow in foams and flowing foams. *Annual Review of Fluid Mechanics*, 45(1):241–267, 2013.

[12] F. P. Bretherton. The motion of long bubbles in tubes. *Journal of Fluid Mechanics*, 10:166–188, 3 1961.

[13] C.-W. Park and G. M. Homsy. Two-phase displacement in hele shaw cells: theory. *Journal of Fluid Mechanics*, 139:291–308, 1984.

[14] I. Cantat. Liquid meniscus friction on a wet plate: Bubbles, lamellae, and foams. *Physics of Fluids*, 25(3):031303, 2013.

[15] N. D. Denkov, V. Subramanian, D. Gurovich, and A. Lips. Wall slip and viscous dissipation in sheared foams: Effect of surface mobility. *Colloids and Surfaces A: Physicochemical and Engineering Aspects*, 263(1):129 – 145, 2005.

[16] C. Raufaste, A. Foulon, and B. Dollet. Dissipation in quasi-two-dimensional flowing foams. *Physics of Fluids*, 21(5):053102, 2009.

[17] S. A. Khan, C. A. Schnepper, and R. C. Armstrong. Foam rheology: III. measurement of shear flow properties. *Journal of Rheology*, 32(1):69–92, 1988.

[18] G. Katgert, B. P. Tighe, M. E. Möbius, and M. van Hecke. Couette flow of two-dimensional foams. *EPL*, 90(5):54002, 6 2010.

[19] A. Maestro, W. Drenckhan, E. Rio, and R. Hohler. Liquid dispersions under gravity: volume fraction profile and osmotic pressure. *Soft Matter*, 9:2531–2540, 2013.

[20] S. A. Koehler, S. Hilgenfeldt, and H. A. Stone. A generalized view of foam drainage: Experiment and theory. *Langmuir*, 16(15):6327–6341, 2000.

[21] N. D. Denkov, S. Tcholakova, K. Golemanov, K. P. Ananthpadmanabhan, and A. Lips. The role of surfactant type and bubble surface mobility in foam rheology. *Soft Matter*, 5:3389–3408, 2009.

[22] E. C. Bingham. An investigation of the law of plastic flow. *Bulletin of the Bureau of Standards*, 13:309–353, 6 1916.

[23] M. Lexis and N. Willenbacher. Yield stress and elasticity of aqueous foams from protein and surfactant solutions – the role of continuous phase viscosity and interfacial properties. *Colloids and Surfaces A: Physicochemical and Engineering Aspects*, 459:177 – 185, 2014.

[24] F. Rouyer, S. Cohen-Addad, and R. Höhler. Is the yield stress of aqueous foam a well-defined quantity? *Colloids and Surfaces A: Physicochemical and Engineering Aspects*, 263(1):111 – 116, 2005.

[25] M. Buchgraber, L. M. Castanier, and A. R. Kovscek. Microvisual investigation of foam flow in ideal fractures: Role of fracture aperture and surface roughness. *SPE Annual Technical Conference and Exhibition*, 1 2012.

[26] C. A. Jimenez-Junca, J. C. Gumy, A. Sher, and K. Niranjan. Rheology of milk foams produced by steam injection. *Journal of Food Science*, 76(9):E569–E575, 2011.

[27] G. M. Campbell and E. Mougeot. Creation and characterisation of aerated food products. *Trends in Food Science & Technology*, 10(9):283 – 296, 1999.

[28] K. Nishinari, M. Turcanu, M. Nakauma, and Y. Fang. Role of fluid cohesiveness in safe swallowing. *NPJ Science of Food*, 3(5), 2019.

[29] S. P. L. Marze, A. Saint-Jalmes, and D. Langevin. Protein and surfactant foams: linear rheology and dilatancy effect. *Colloids and Surfaces A: Physicochemical and Engineering Aspects*, 263(1):121 – 128, 2005.

[30] G. K. Essick, A. Chopra, S. Guest, and F. McGlone. Lingual tactile acuity, taste perception, and the density and diameter of fungiform papillae in female subjects. *Physiology & Behavior*, 80(2):289 – 302, 2003.

[31] E. A. Foegeding, C. J. Vinyard, G. Essick, S. Guest, and C. Campbell. Transforming structural breakdown into sensory perception of texture. *Journal of Texture Studies*, 46(3):152–170, 2015.

[32] B. Linne and C. T. Simons. Quantification of oral roughness perception and comparison with mechanism of astringency perception. *Chemical Senses*, 42(7):525–535, 06 2017.

Supplementary Materials
Roughness-induced friction in liquid foams

Manon Marchand[1], Frédéric Restagno[1], Emmanuelle Rio[1], and François Boulogne[1]

[1]Université Paris-Saclay, CNRS, Laboratoire de Physique des Solides, 91405, Orsay, France

1 Material

Preparation of the probing surfaces

Smooth surfaces are microscope glass slides (Ted Pella, $75 \times 25 \times 1$ mm). Model rough surfaces are made by gluing glass beads (Wheelabrador) with a thin layer of epoxy glue in a random packing fashion on the same glass slides. The mean radius a of the glass beads is measured from the particle size distribution obtained with a microscope (Keyence VHX -S90BE, and varies in the range $0.030 - 0.44$ mm (Fig. S1). All surfaces, rough or smooth, are prewetted with the soap solution prior each experiment to prevent bubble rupture [1].

(a)

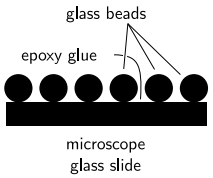

(b)

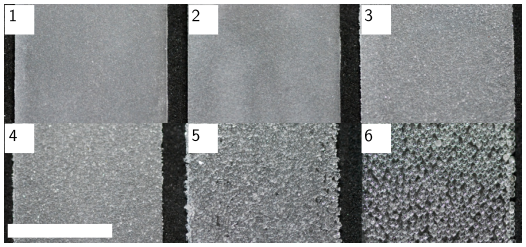

(c)

number	1	2	3	4	5	6
a (μm)	30	40	78	125	225	440
δa (μm)	6	9	38	53	65	34

Figure S1: Patterned surfaces **a**, Cross-section of a patterned surface made by gluing glass beads in a random packing organization on a microscope glass slide. **b**, Images (Nikon D60, 105mm Ex sigma DG Macro) of the six patterned surfaces used in this study, the scale bar is 2 cm. **c**, Table presenting the mean value and values of the standard deviation for the beads radii a.

Container and foam production

The foam container is filled partially with a soap solution, and we blow air at a controlled pressure (Elveflow AFI-1600-8317) through eight needles (Nordson EFG 32G) that perforate the bottom of the container. The bubbles produced through the needles rise and form a foam on top of the soap solution, their radius is $R = 0.70 \pm 0.05$ mm. The soap solution is made of pure deionized water at 18.2 MΩ·cm produced in the laboratory (PureLab Chlorus 1 ELGA, Veolia) and 10 % vol. professional Fairy dishwashing liquid. Its surface tension $\gamma = 25.4 \pm 0.1$ mN/m is measured with a Wilhelmy tensiometer (Kibron EZ-PI+), and its viscosity $\mu = 1.0 \pm 0.2$ mPa·s is measured with a rheometer (Anton Paar MCR 302) in a double gap geometry (Anton Paar DG 26.7). The liquid fractions φ_ℓ of the foam can be varied between 0.03 and 8 % by changing the working height above the liquid-foam interface [2] (Fig. S2). For such dry foams, the radius of curvature of the intersection between three bubbles, which is called a Plateau border, is given by $r_{\rm pb} = R\sqrt{\varphi_\ell/0.33}$ [3]. In our experiment, it varies in the range $r_{\rm pb} = 0.02 - 0.4$ mm. When the foam reaches the top of the container, we cover it with a large microscope glass slide (Ted Pella, $152 \times 114 \times 1$ mm) to prevent evaporation.

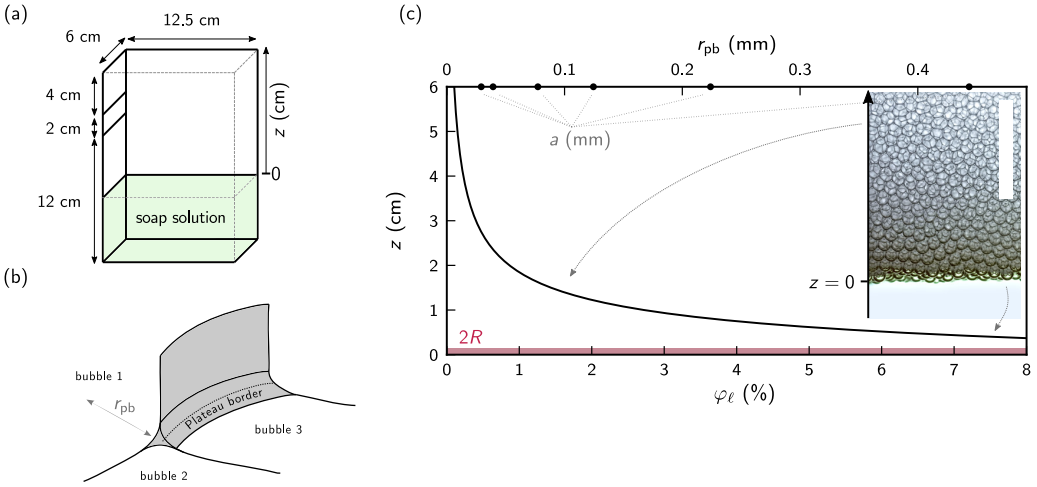

Figure S2: Foam generation and characterization **a**, Dimensions of the container in which the foam is produced by blowing air in the soap solution. The height of foam between the level of the soap solution and the probing surface is changed by adjusting the volume of soap solution at the bottom of the container. **b**, The intersection between three bubbles is a Plateau border. It is characterized by a radius of curvature $r_{\rm pb}$. **c**, Plot of the semi-empirical equation from [2] for the liquid fraction profile of a foam. The plot represents the height of foam z as a function of the liquid fraction φ_ℓ and of the radius of curvature of the Plateau borders $r_{\rm pb}$. The mean beads sizes are indicated on the top axis. The bubble diameter $2R$ is represented at the bottom to scale the vertical axis. The insert is a picture (Nikon D7200, with a Nikon 200 mm objective) of a foam on a liquid bath for which the gradient of liquid fraction is visible. The scale bar is 1 cm.

Foam characterization

The size of the bubbles $R = 0.70 \pm 0.05$ mm is measured by recording a video (Photron Fastcam SA3, working at 125 frames per second) while the bubbles rise in the soap solution after their formation, and measuring the bubble size distribution with ImageJ. This radius is a constant for this study.

To change the liquid fraction φ_ℓ in the foam, we use the semi-empirical equation derived by [2]. This equation provides the dependency of the liquid fraction as a function of the height of foam above a liquid pool, and is plotted in Fig. S2. To change the foam height between the surface of the liquid and the probing surface, we fill the container with different volumes of soap solution. In our conditions, the liquid fractions vary between 0.03 % and 8 %. For such dry foams, the radius of curvature of the Plateau borders is calculated from the equation $r_{\rm pb} = R\sqrt{\varphi_\ell/0.33}$ [3], and varies between 0.02 and 0.4 mm. The range of variation in curvature radius of the Plateau borders $r_{\rm pb}$ is chosen such as there is an overlapping in $a/r_{\rm pb}$ between the different beads sizes (Fig. S4c).

2 Methods

Visualization

We record the motion of the Plateau borders in the foam close to the rough surfaces with a camera (Basler acA3800 14 μm) and a telecentric objective (Techspec 0.73× GoldTL). The videos are captured through the observation side of the foam container, and the focus is made on Plateau borders two bubbles away from the wall, to avoid probing two dimensional effects

due to the wall closeness. The position of the Plateau borders, as presented in Fig 1, on the surfaces are detected manually and are only useful for an estimation of the limits between the different friction regimes.

Motion and force sensor

With a translation stage (Thorlabs LTS300/M), we insert the different rough surfaces in the foam at constant velocities V from 0.5 to 20 mm/s, corresponding to capillary numbers Ca in the range 1.7×10^{-5} to 6.7×10^{-4}.

A capacitive sensor (Fogale Nanotech CS200) detects the displacement of two parallel beryllium copper (Weber Métaux) cantilever springs, as described in [4]. Each spring has a 4 cm^2 effective surface, and a 0.31 mm thickness. The calibration is realized by adding calibrated weights on the double spring system, and we check that the behavior of the springs is linear for the probed forces (Fig. S3). With this setup, we can probe forces between 0.1 and 200 mN with a 0.05 mN uncertainty, every 0.05 s. For the experiment, a probing surface is attached to the force sensor. The foam container is then approached with a translation stage (Thorlabs LTS300/M) at constant velocities between 0.5 and 20 mm/s. Raw measurements give the force exerted by the foam on the probing surface as a function of time and position, as plotted in Fig 1c.

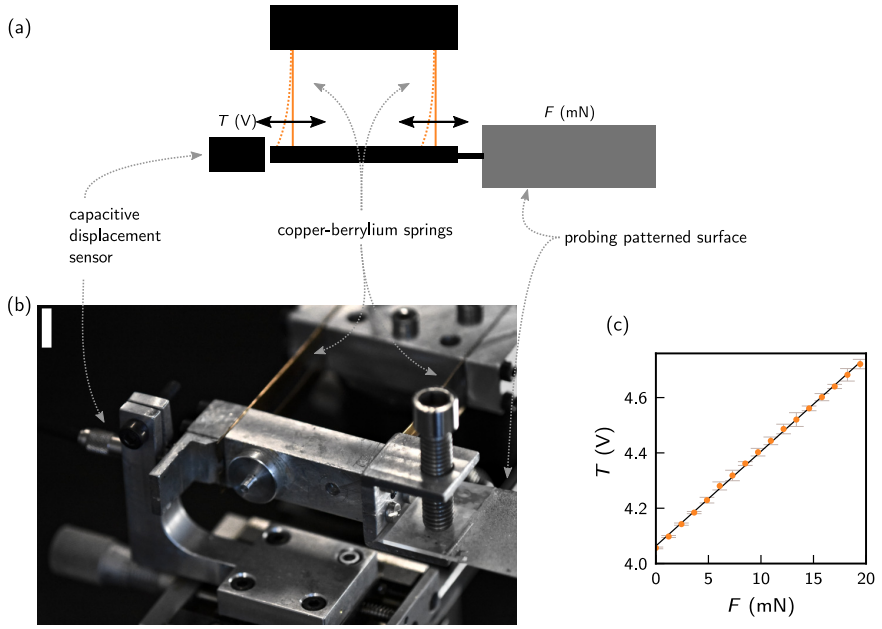

Figure S3: Force measurements **a**, Top view schematics of a force sensor made with two copper-beryllium springs. When a force is exerted on the patterned surface, the springs deform linearly, and a capacitive displacement sensor detects the motion. **b** Photograph of the force sensor (Nikon D7200, with a Nikon 200 mm objective). The scale bar is 1 cm. **c**, Calibration curve of the displacement sensor obtained by adding calibrated weights. The force sensor has a linear behavior and the error bars are due to the fluctuations, estimated from a standard deviation over one minute.

Renormalisation of the roughness size

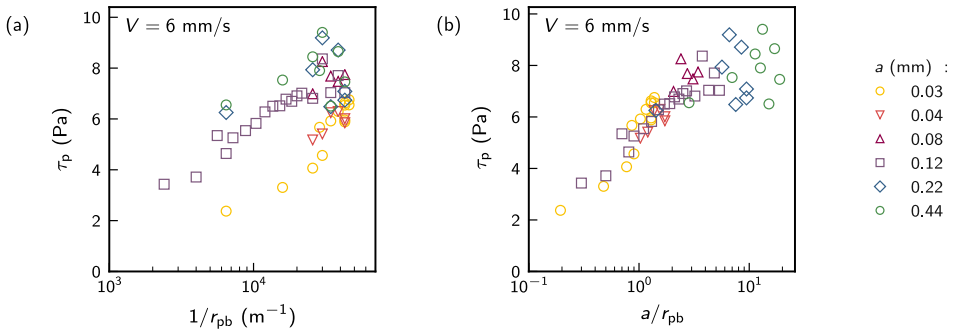

Figure S4: Roughness factor definition (a) Stress in the stick-slip and anchored regimes for a given velocity $V = 6$ mm/s and different liquid fractions φ_ℓ, as a function of $1/r_{\rm pb} \propto 1/\sqrt{\varphi_\ell}$. The different symbols represent the different beads sizes a. For a unique curvature radius $r_{\rm pb}$, different beads sizes lead to different measured stresses. (b) Representation of the data set in (a), as a function of $a/r_{\rm pb}$. The data collapses: a single roughness factor $a/r_{\rm pb}$ gives the same stress measurement independently of the bead size.

Bingham number estimation

When sheared above its yield stress $\tau_{\rm ys}$, the foam rheological behavior is described by an Hershell-Bulkley law $\tau_{\rm HB} = \tau_{\rm ys} + \eta(\dot\gamma)\dot\gamma$ [5]. The Bingham number ${\rm Bi} = \tau_{\rm ys}/\eta(\dot\gamma)\dot\gamma$ compares the yield stress to the viscous stresses contributions in this law [6]. An estimate of the order of magnitude of the foam viscosity close to the yield point gives $\eta \sim 10$ Pa·s [7]. Velocities in the range 0.5 to 20 mm/s are imposed to the system. The shearing distance $\delta \sim 1$ cm is estimated by visual observation of the distance of propagation of plastic events. This gives shear rates $\dot\gamma = V/\delta$ in the range 0.05 to 2 s^{-1}. The yield stress of the foam $\tau_{\rm ys} = 7.0 \pm 0.7$ Pa is given by equation (2). Thus, the maximum values for the Bingham number are ${\rm Bi} \sim 0.3$ for the faster imposed velocities, and ${\rm Bi} \sim 10$ for the slower ones.

Stress derivation

As a surface is inserted in a foam, our measurements indicate that the force increases linearly in time (Fig. 1c), and is a linear function of the displacement since the velocity is constant. For the surfaces that are identical on both sides, either bare or decorated with asperities, the force writes $F(t) = \tau_{\rm p} 2p(t)d$, where $p(t)$ is the penetration length of the surface that increases linearly with time, $d = 2.5$ cm is the perpendicular dimension of the probing surface, and the factor 2 stands for the two sides of the surface.

We also used surfaces composed of a bare side and a decorated with asperities side. Therefore, the total force is the sum of the contributions of two surface types. On the bare side, the contribution of the sliding stresses $\tau_{\rm slip}$ is set by the equation (1). Thus the total force writes $F(t) = \tau_{\rm p} p(t)d + \tau_{\rm slip} p(t)d$. We checked experimentally that the two configurations give equivalent stress measurements as shown in the Fig. S5.

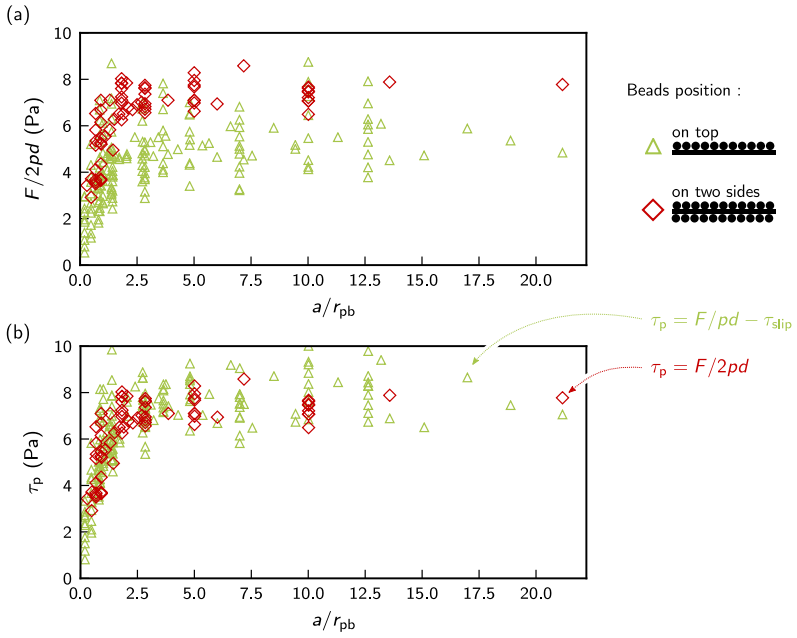

Figure S5: Stress derivation (a) Plot of the ratio $F/2pd$ as a function of a/r_{pb} for the two types of rough surfaces used in this study. The green triangles represent surfaces for which the asperities are only on the top side, and the red diamonds represent the asperities on both sides. (b) Plot of the contribution of the rough sides to the stress τ_{p}, as defined in Methods, as a function of a/r_{pb}, for the two types of probing surfaces. The collapse of the two sets of data validates the description of the stress τ_p as the contribution of the foam on the rough surface.

Determination of the prefactor k between the stick-slip and the anchored regimes

We define a reduced chi-squared $\chi^2 = \frac{1}{N}\sum_i^N \mathrm{Res_i}^2$, where N is the number of data points in the stick-slip regime that we extract from the data set of the Fig. 2a, and Res is the residual between the equation (3) and the data sets without any fitting parameter. We plot χ^2 for different data sets corresponding to different transition values k_{imposed} in the Fig. S6a.

The smallest value of the χ^2 is obtained for $k = 1.9 \pm 0.2$, where the uncertainty comes from the sampling around the transition, and from the uncertainty of the yield stress value τ_{ys} calculated from the equation (2) and the mean of our data in the anchored regime.

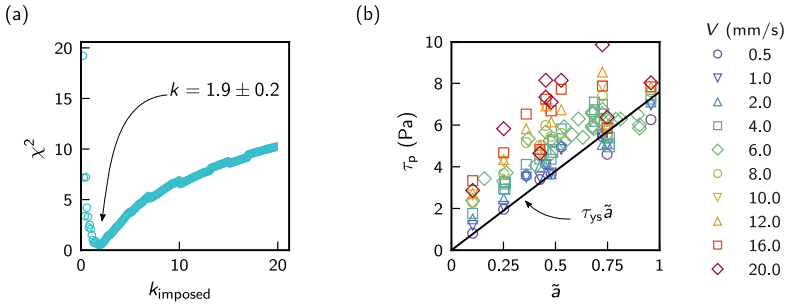

Figure S6: Stick-slip regime (a) Plot of the reduced χ^2 as a function of the imposed transition k_{imposed} for different data sets, as described in the Methods section. The minimum χ^2 is obtained for $k = 1.9 \pm 0.2$. (b) Experimental data for the stick-slip regime conditions. We represent the stress τ_{p} during the motion of rough probes in foam, as a function of the transition $\tilde{a} = a/kr_{\mathrm{pb}}$ for the same data set than in Fig. 2. The data dispersion highlights the role of the velocity in this regime. The stress for the lower velocities follows the prediction $\tau_{\mathrm{ys}}\tilde{a}$.

Complementary representations of Figure 2a

The full data set discussed in the article is presented in the Figure 2a, in which we chose to highlight the different friction regimes. Here, we provide a representation of the data in the stick-slip and the anchored regimes that offers a more complete view of the influence of either the asperity size a or the velocity V.

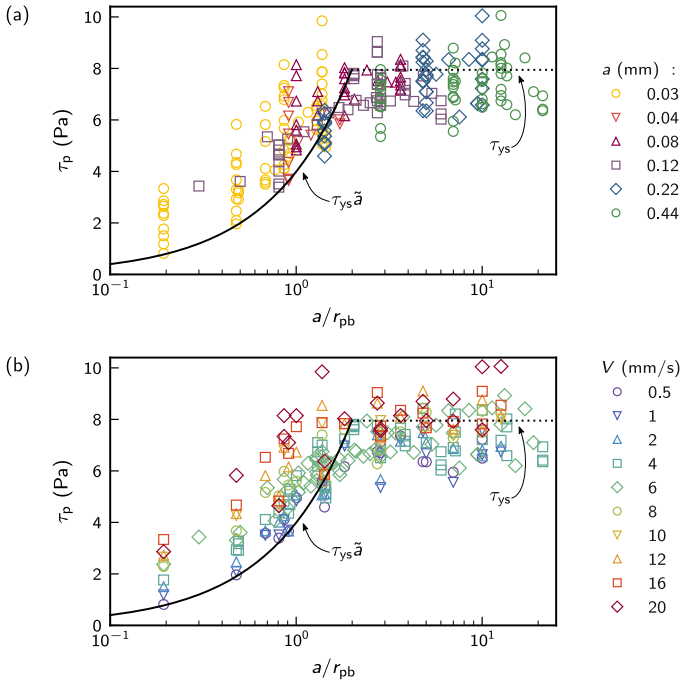

Figure S7: Complementary representations of Figure 2a. (a) Stresses τ_p as a function of the roughness factor a/r_{pb}. The different colors highlight the different asperities sizes on the probing surfaces. We remark here that a same roughness can lead to different slip regimes depending of the curvature radius of the Plateau borders r_{pb}. (b) Stresses τ_p as a function of the roughness factor a/r_{pb}. The different colors highlight the different velocities of the probing surfaces.

3 Supplementary movies

Flow of foams near surfaces

Movie S1 Liquid foam on a smooth glass plate moving at $V = 1$ mm/s in the right to left direction. The foam is not sheared by the motion of the plate.
Movie S2 Liquid foam on a glass plate decorated with beads of radii $a = 0.030 \pm 0.006$ mm. The plate is moving from right to left at $V = 1$ mm/s. The Plateau borders in contact with the rough surface present a stick-slip motion.
Movie S3 Liquid foam on a glass plate decorated with beads of radii $a = 0.44 \pm 0.03$ mm. The plate is moving from right to left at $V = 1$ mm/s. The Plateau borders are pinned on the beads, and the stress is dissipated by plastic events.

Tuning foam properties to change the perceived texture

Albumen foams sheared between a table spoon moving at 10 mm/s and a static glass surface covered with beads of mean radius $a = 225$ μm, modeling a human tongue.

Movie S4 Case of a wet foam with $\varphi_\ell \simeq 0.7$ %, corresponding to a roughness factor $\tilde{a} \sim 0.5$. The foam slides on the model tongue.
Movie S5 Case of a dryer foam with a liquid fraction $\varphi_\ell \simeq 0.02$ %, meaning $\tilde{a} \simeq 3$. The foam is anchored on the model tongue.

References

[1] P. M. Ireland and G. J. Jameson. Drag force on a spherical particle moving through a foam: The role of wettability. *International Journal of Mineral Processing*, 102-103:78 – 88, 2012.

[2] A. Maestro, W. Drenckhan, E. Rio, and R. Hohler. Liquid dispersions under gravity: volume fraction profile and osmotic pressure. *Soft Matter*, 9:2531–2540, 2013.

[3] S. A. Koehler, S. Hilgenfeldt, and H. A. Stone. A generalized view of foam drainage: Experiment and theory. *Langmuir*, 16(15):6327–6341, 2000.

[4] F. Restagno, J. Crassous, E. Charlaix, and M. Monchanin. A new capacitive sensor for displacement measurement in a surface-force apparatus. *Measurement Science and Technology*, 12(1):16, 2001.

[5] N. D. Denkov, S. Tcholakova, K. Golemanov, K. P. Ananthpadmanabhan, and A. Lips. The role of surfactant type and bubble surface mobility in foam rheology. *Soft Matter*, 5:3389–3408, 2009.

[6] E. C. Bingham. An investigation of the law of plastic flow. *Bulletin of the Bureau of Standards*, 13:309–353, 6 1916.

[7] S. P. L. Marze, A. Saint-Jalmes, and D. Langevin. Protein and surfactant foams: linear rheology and dilatancy effect. *Colloids and Surfaces A: Physicochemical and Engineering Aspects*, 263(1):121 – 128, 2005.